Dalton Transactions

Alkyl Pyridinium Iodocyanocuprate(I) Chains $(RPy)_2[Cu_2I_3(CN)]$: Insight into Structural, Electronic and Spectroscopic Properties

Journal:	*Dalton Transactions*
Manuscript ID	DT-ART-11-2019-004340.R1
Article Type:	Paper
Date Submitted by the Author:	19-Dec-2019
Complete List of Authors:	Pike, Robert; College of William & Mary, Chemistry Well, Taylor; College of William & Mary, Chemistry Streep, Michaela; College of William & Mary, Chemistry Martucci, Abigail; College of William & Mary, Chemistry Nicholas, Aaron; George Washington University, Chemistry

ARTICLE

Alkyl Pyridinium Iodocyanocuprate(I) Chains $(RPy)_2[Cu_2I_3(CN)]$: Insight into Structural, Electronic and Spectroscopic Properties

Received 00th January 20xx,
Accepted 00th January 20xx

DOI: 10.1039/x0xx00000x

Taylor C. Wells,[a] Michaela E. Streep,[a] Abigail L. Martucci,[a] Aaron D. Nicholas,[b]* Robert D. Pike[a]*

Equimolar mixtures of copper(I) iodide (CuI) and copper(I) cyanide (CuCN) react with N-alkyl pyridinium iodides (RPy^+I^-, R = Me, Et, *n*-propyl = Pr, and *n*-butyl = Bu) to produce pyridinium iodocyanocuprate(I) salts, $(RPy)_2[Cu_2I_3CN]$. Crystal structures reveal isostructural anionic chains consisting of trigonal pyramidal $Cu_2(\mu_2\text{-}I)_3$ clusters bridged by C/N-disordered cyano units. The 1-D chains are nearly linear but vary with respect to whether adjacent clusters are staggered or eclipsed. A detailed investigation via Hirshfeld surface analysis reveals that hydrogen bonding between the triiodide group and pyridinium cation are the driver for assembly in these systems. Interestingly, spectroscopic investigations of absorption edge and emission energies show a general red shift with increasing hydrogen bonding. DFT and TD-DFT calculations were used to determine the electronic structure and band assignment of these materials to elucidate the nature behind this structure/function relationship.

1. Introduction

Anionic metal halide clusters, particularly those of d^{10} and post-transition metals, show remarkable structural diversity and are of interest for their electronic and photophysical properties.[1] Of special interest are copper(I) and the univalent group 11 metals, which offer variable coordination number, relative softness, and diverse photoemissive behaviours.[2,3] A vast body of literature on iodocuprate(I) clusters, $[Cu_yI_{x+y}]^{x-}$, shows remarkable structural diversity, consisting of secondary building units (SBUs) ranging from zero- (molecular) to one-, two-, and three-dimensional clusters.[4] Iodocuprates may be network or molecular, with cluster size varying tremendously, ranging from $[Cu_2I_3]^-$ up to $[Cu_{36}I_{56}]^{20-}$. Cyanocuprate(I) compounds are known for a variety of cations.[5] In contrast to iodocuprates, the linear CN^- ion strongly favors sheet and net formation. Particularly common is the 2-D $[Cu_2(CN)_3]^-$ network consisting of tiled $Cu_6(CN)_6$ hexagons sharing trigonal planar Cu(I) nodes. Thus, while halides, particularly iodide, tend to produce metal clusters through acute angle bridging, cyanide favors linear bridges between metal centres. Materials that utilize both iodide and cyanide in controlled ratios could, at least in theory, produce a "molecular wire." In this putative chain, electron reservoir copper iodide clusters would be bridged to form infinite chains by cyano groups, allowing electronic communication between clusters.

Reports of halocyanocuprates(I) of formula $[Cu_aX_b(CN)_c]^{(b+c-a)-}$ in the literature are relatively few. Examples include $(Bu_4N)[CuXCN]$ (X = Br, I) prepared in refluxing acetone.[6] These compounds consist of zigzag CuCN chains with the 3-coordinate copper centres decorated with terminal halide ligands. Also reported are various alkali metal salts from hydro- or solventothermal reactions: $K[Cu_2(CN)_2Br]\cdot H_2O$, $K_3[Cu_6(CN)_6I_3]\cdot 2H_2O$, $Cs[Cu_3(CN)_3Cl]$, $Cs[Cu_3(CN)_3Br]$ and $Cs_2[Cu_4(CN)_4I_2]\cdot H_2O$,[7] and $[Me_4N][Cu_3(CN)_2Br_2]$ and $[Me_4N]_2[Cu_4(CN)_5Cl]$.[8] All reported iodocyanocuprates have been found to be 1-, 2-, or 3-D networks. This behaviour is the result of the bridging ability of the cyano unit, and stands in contrast to halocuprates which sometimes form as isolated clusters. Recently, a particularly rich array of iodocyanocuprates was reported by Zhai and coworkers.[9] Reaction of CuCN at 120 °C in various alkylimidazolium halide ionic liquids produced alkylimidazolium salts containing the following anions: $[Cu_2X_3(CN)]^{2-}$ (X = Br, I), $[Cu_5ClI_2(CN)_4]^{2-}$, and $[Cu_4I(CN)_4]^-$, along with several novel iodocuprates and cyanocuprates. These imidazolium halocyanocuprates exhibited strong photoluminescence and are potentially semiconductive owing to their small optical band gaps. Despite these promising properties, the underlying photophysical behaviour for these materials is not fully understood.

In our previous study of the closely related pyridinium iodocuprates, the products of reactions (1) and (2) did not show the simple formula $(RPy)[CuI_2]$.[10] Instead, an array of CuI-rich products were formed according to reaction (3). These included: $(HPy)_3[Cu_3I_6]$, $(MePy)[Cu_2I_3]$, $(EtPy)[Cu_3I_4]$, $(PrPy)_2[Cu_6I_8]$, and $(RPy)_2[Cu_5I_7]$, R = n-butyl (Bu), n-pentyl (Pn), and n-hexyl (Hx). All of these anions are polymeric, either 1- or 2-D. Charge transfer behaviour between the iodocuprate anions and the arylinium cations was observed in this series, along with cluster-centred halide-to-metal charge transfer; nevertheless,

[a] Department of Chemistry, College of William and Mary, Williamsburg, VA 23187 USA.
[b] Department of Chemistry, George Washington University, Washington, DC 20052 USA.

† Electronic supplementary information (ESI) available: Crystallographic data, additional structural figures and descriptions, IR spectra, and PXRD patterns. CCDC 1964373–1964376 for **1–4**. For ESI and crystallographic data in CIF or other electronic format see. See DOI: 10.1039/x0xx00000x

the photophysical interpretation was complicated by the structural diversity across the series.

$$Py + RI \rightarrow RPyI \quad (1)$$

$$RPyI + CuI \rightarrow (RPy)[CuI_2] \quad (2)$$

$$x\ RPyI + y\ CuI \rightarrow (RPy)_x[Cu_yI_{x+y}] \quad (3)$$

Given the relative paucity of study of iodocyanocuprates and expecting a greater degree of structural consistency for these anions, such as was observed in the alkylimidazolium halocyanocuprates,[9] we set out to prepare a series of iodocyanocuprate(I) anions paired with alkylpyridinium cations. We speculated that an isostructural series of anions might accompany simple alkyl group changes in the pyridinium series permitting a systematical exploration of cation dependence towards structural assembly and spectroscopic properties. As described herein, we have successfully prepared and studied the alkylpyridinium iodocyanocuprate(I) series $(RPy)_2[Cu_2I_3CN]$ (R = Me, Et, Pr, Bu) and identified charge transfer behaviour.

2. Experimental Section

2.1 General

All reagents were purchased from Aldrich or Acros. Acetone was dried by distilling from Drierite and THF was dried by distilling from Na/benzophenone ketyl. Other reagents and solvents were used as received. Pyridinium iodide compounds were prepared as previously described.[10]

2.2 Syntheses of 1–4

*$\{(MePy)_2[Cu_2I_3CN]\}_\infty$ (**1**):* [MePy]I (88.4 mg, 0.400 mmol) and KI (16.6 mg, 0.100 mmol) were dissolved in 5 mL acetone to form a yellow solution. CuI (38.1 mg, 0.200 mmol) and CuCN (17.9 mg, 0.200 mmol) were added, forming a yellow suspension, which was flushed with Ar and sealed in a pressure tube. The mixture was heated to 70 °C with stirring overnight. Frequent agitation was required to re-suspend the solid. The resulting orange powder was collected via decantation, washed with ethyl ether, and dried overnight under vacuum: 90.0 mg, 0.125 mmol, 62.3%. Anal. Calcd for $C_{13}H_{16}Cu_2I_3N_3$: C, 21.62; H, 2.23; N, 5.82. Found: C, 22.15; H, 2.17; N, 5.54.

*$\{(EtPy)_2[Cu_2I_3CN]\}_\infty$ (**2**):* [EtPy]I (71.0 mg, 0.302 mmol) and KI (12.0 mg, 0.0723 mmol) were dissolved in 5 mL acetone to form a yellow solution. CuI (29.0 mg, 0.152 mmol) and CuCN (13.0 mg, 0.145 mmol) were added, forming a yellow suspension, which was flushed with Ar and sealed in a pressure tube. The mixture was heated to 70 °C with stirring overnight. Frequent agitation was required to re-suspend the solid. The resulting yellow powder was collected via decantation, washed with ethyl ether, and dried overnight under vacuum: 61.0 mg, 0.0813 mmol, 56.1%. Anal. Calcd for $C_{15}H_{20}Cu_2I_3N_3$: C, 24.02; H, 2.68; N, 5.60. Found: C, 24.26; H, 2.54; N, 5.73.

*$\{(PrPy)_2[Cu_2I_3CN]\}_\infty$ (**3**):* [PrPy]I (1010 mg, 0.405 mmol) and KI (16.8 mg, 0.101 mmol) were dissolved in 5 mL acetone to form a yellow solution. CuI (38.6 mg, 0.203 mmol) and CuCN (18.1 mg, 0.203 mmol) were added, forming a yellow suspension, which was flushed with Ar and sealed in a pressure tube. The mixture was heated to 70 °C with stirring overnight. Frequent agitation was required to re-suspend the solid. The resulting yellow powder was collected via decantation, washed with ethyl ether, and dried overnight under vacuum: 103.0 mg, 0.132 mmol, 65.4%. Anal. Calcd for $C_{17}H_{24}Cu_2I_3N_3$: C, 26.24; H, 3.11; N, 5.40. Found: C, 26.35; H, 2.95; N, 5.36.

*$\{(BuPy)_2[Cu_2I_3CN]\}_\infty$ (**4**):* [BuPy]I (78.9 mg, 0.300 mmol) and KI (12.0 mg, 0.0723 mmol) were dissolved in 7 mL THF to form a yellow solution. CuI (28.6 mg, 0.150 mmol) and CuCN (13.4 mg, 0.150 mmol) were added, forming a yellow suspension, which was flushed with Ar and sealed in a pressure tube. The mixture was heated to 70 °C with stirring overnight. Frequent agitation was required to re-suspend the solid. The resulting yellow powder was collected via decantation, washed with ethyl ether, and dried overnight under vacuum: 97.0 mg, 0.120 mmol, 80.2%. Anal. Calcd for $C_{19}H_{28}Cu_2I_3N_3$: C, 28.31; H, 3.50; N, 5.21. Found: C, 28.06; H, 3.36; N, 5.07.

2.3 X-ray crystallography

Crystals were grown by carrying out the reactions described above without stirring or agitation. Crystals were mounted on glass fibers. All measurements were made using graphite-monochromated Mo (**1**–**3**) or microfocus Cu (**4**) Kα radiation on a Bruker-AXS DUO three-circle diffractometer, equipped with an Apex II CCD detector. Initial space group determination was based on a matrix consisting of 36 or 120 frames. The data were reduced using SAINT+,[11] and empirical absorption correction applied using SADABS.[12] Structures were solved using intrinsic phasing. Least-squares refinement for all structures was carried out on F^2. The non-hydrogen atoms were refined anisotropically. Hydrogen atoms were placed in riding positions and refined isotropically. Structure solution, refinement, and the calculation of derived results were performed using the SHELXTL package of computer programs[13] and ShelXle.[14]

2.4 Photophysical measurements

Diffuse reflectance spectra were collected on microcrystalline samples of **1**–**4** at 298 K. The light source was a Mikropack DH-2000-BAL deuterium and halogen light source coupled with an Ocean Optics Flame detector. Scattered light was collected with a fiber optic cable. Spectra were referenced with $MgSO_4$. Data were processed using OceanView spectroscopy software. Steady-state luminescence scans of **1**–**4** were collected at 298 K and 78 K. Spectra were collected with a Fluorolog-3 photoluminescence spectrophotometer from Horiba using a 450 W xenon arc lamp combined with double excitation and double emission monochromators. A photomultiplier tube at 950 V was used as the emission detector. For low temperature measurements solid samples were placed in a quartz NMR tube, which was capped, and submerged in a quartz Dewar filled with liquid nitrogen. Lifetime measurements were performed using a Horiba Jobin Yvon Fluorolog-3 spectrometer adapted for time-correlated single photon counting (TCSPC) and multichannel scaling (MS) measurements using a xenon flash lamp as a light source. Lifetime profiles were obtained using the Jobin Yvon Fluorohub single photon counting module.

2.5 Molecular modelling and Hirschfeld analysis

Density Functional Theory (DFT) calculations were performed on models of **1–4** to investigate photophysical properties using the Gaussian 16 software (Gaussian Inc.) with the University of Maine Advanced Computing Group.[15] Ground state calculations were performed on models using the B3LYP[16] functional with the modified scalar-relativistic effective core potential (ECP) basis set LANL2DZ[17] as implemented in the software. Experimental X-ray data were used as initial input to develop models for **1–4**. Calculations were performed on a cationic subunit with formula $(RPy)_4[Cu_4I_6(CN)_3H_2]$ (R = Me, Et, Pr, Bu). Hydrogen atoms were used to cap the infinite $[Cu_2I_3(CN)_2]^{3-}$ chains at the pendent C/N position and thus reduce the available degrees of freedom of the terminal CN ligands. The models maintain the local tetrahedral geometry of the Cu(I) coordination spheres and account for the close measured Cu···Cu distances. Deviations in bond lengths/angles are considered minor and are attributed to lack of crystal packing effects in the model, especially with regard to the rotation of the pyridinium cations. The agreement between experimental observations and ground state parameters (see Electronic Supplementary Information) supports our models as accurately describing the photophysical behaviour observed. Isodensity representations of molecular orbitals were visualized using the Avogadro 1.2.0 software program.[18] Hirshfeld surfaces were generated for the anionic iodocyanocuprate backbones of **1**–**4** to evaluate and compare the noncovalent interactions present in each complex. To generate these surfaces, isolated anions of truncated formula $[(Cu_2I_3)_3(CN)_4]$ were selected, along with surrounding pyridinium cations. Three-dimensional Hirshfeld surfaces were generated with an isovalue of 0.5 au using CrystalExplorer as implemented in the software.[19] Surfaces were rendered as 2D fingerprint plots and delineated by atom···atom type.

3. Results and discussion

3.1 Synthesis

There have been few reported syntheses of halocyanocuprates. The majority of these were carried out under heterogeneous conditions with solid present in solvent suspension at elevated temperatures, at or above the solvent boiling point. In these reactions, insoluble CuCN is heated in a solution of halide salt, allowing thermodynamic stability of the crystalline phase to control the formation of a particular product. The intended product series in the present study was $(RPy)_2[Cu_2I_3CN]$, R = Me (**1**), Et (**2**), Pr (**3**), and Bu (**4**). Thus, in an effort to obtain the 1-D polymer $\{[Cu_2I_3CN]^{2-}\}_\infty$ paired with RPy^+, a 2:1:1 ratio between RPyI, CuCN, and CuI was employed, reaction (4).

$$2\ RPyI + CuCN + CuI \rightarrow (RPy)_2[Cu_2I_3CN] \quad (4)$$

The use of two insoluble Cu(I) salts made identification of conditions that would yield the desired product fairly challenging. Use of hydrogen-bonding solvents, such as water and alcohols at 70 °C, resulted in Cu, C, and N mass percents above what would be expected. Thus, in these cases

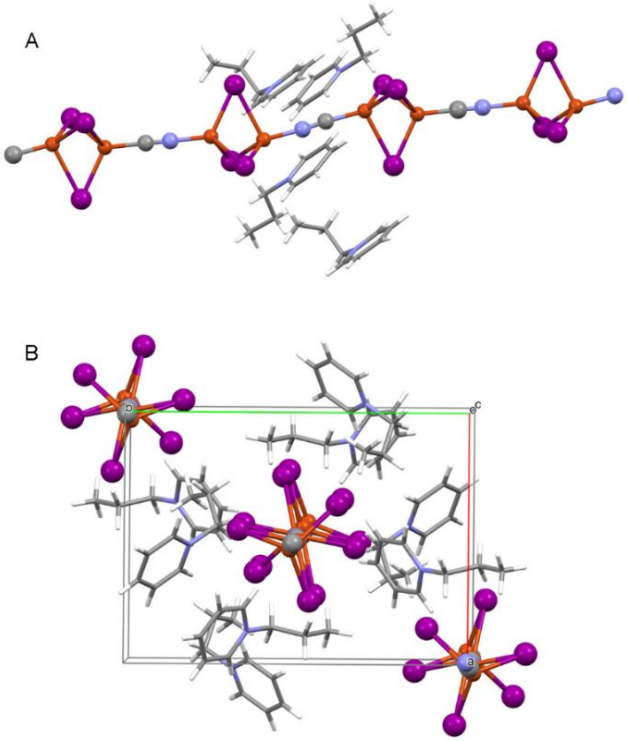

Figure 1. X-ray structure of **1**, anion shown as ball and stick, cation shown as wireframe. A: chain structure; B: unit cell viewed down *a*-axis. Colour scheme: orange = Cu, purple = I, grey = C, blue = N.

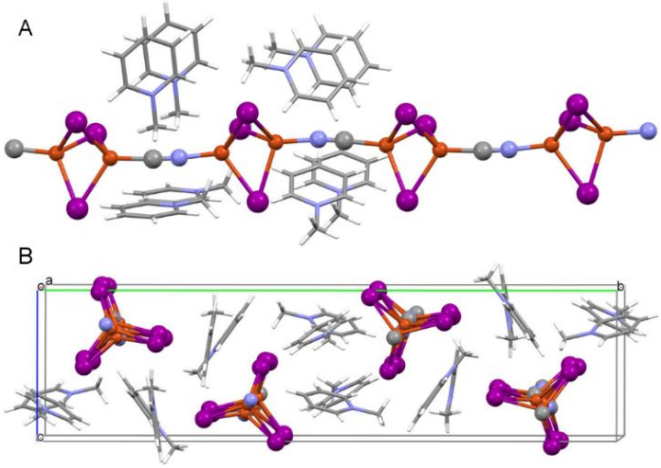

Figure 2. X-ray structure of **3**, anion shown as ball and stick, cation shown as wireframe. A: chain structure; B: unit cell viewed down *c*-axis. Colour scheme: orange = Cu, purple = I, grey = C, blue = N.

cyanocuprates were primarily being formed, with much of the iodide remaining in solution. Polar aprotic solvents, particularly acetone and THF at 70 °C, gave improved analyses for products **1–4**. To optimize analytical and powder X-ray diffraction (PXRD) results, the addition of one half equivalent of KI in acetone was found to be optimal for preparation of **1**–**3**. Nevertheless, R = Bu product **4** still gave elevated percent Cu under these conditions. The use of THF solvent and one half equivalent of KI allowed for analytically pure $(BuPy)_2[Cu_2I_3CN]$, **4**.

Table 1. Crystal and Structure Refinement Data.

	1	**2**	**3**	**4**
CCDC deposit no.	1964373	1964374	1964375	1964374
colour and habit	orange prism	yellow prism	yellow prism	orange prism
size, mm	0.21 × 0.10 × 0.08	0.34 × 0.09 × 0.06	0.53 × 0.08 × 0.05	0.25 × 0.12 × 0.09
Formula	$C_{26}H_{32}Cu_4I_6N_6$	$C_{15}H_{20}Cu_2I_3N_3$	$C_{17}H_{24}Cu_2I_3N_3$	$C_{19}H_{28}Cu_2I_3N_3$
formula weight	1444.13	750.12	778.17	806.22
space group	$P2_1/c$	$C2/c$	$P2_1/n$	$P2_1/c$
a, Å	14.6496(6)	14.3925(7)	10.8148(14)	14.8955(4)
b, Å	31.7022(12)	16.2544(8)	14.4485(19)	8.8088(3)
c, Å	8.2725(3)	9.1907(6)	14.7668(19)	20.4146(6)
β, deg	94.5140(10)	105.1840(10)	102.129(2)	109.9220(10)
volume, Å^3	3830.0(3)	2075.0(2)	2255.9(5)	2518.33(13)
Z	4	4	4	4
ρ_{calc}, g cm^{-3}	2.504	2.401	2.291	2.126
F_{000}	2656	1392	1456	1520
μ(Mo Kα), mm^{-1}	7.053	6.514	5.997	31.018[b]
Temp., K	100	100	100	100
residuals:[a] R; R_w	0.0226, 0.0449	0.0147, 0.0315	0.0185, 0.0376	0.0338, 0.0827
goodness of fit	1.149	1.074	1.027	1.198
peak and hole, eÅ^{-3}	0.739, –0.429	0.542, –0.368	0.572 –0.461	0.594, –0.788

[a]$R = R_1 = \Sigma||F_o| - |F_c||/\Sigma|F_o|$ for observed data only. $R_w = wR_2 = \{\Sigma[w(F_o^2 - F_c^2)^2]/\Sigma[w(F_o^2)^2]\}^{1/2}$ for all data. [b]Cu Kα.

Table 2. Selected bond lengths (Å) and angles (°).[a]

	Cu–I	**Cu–X**	**X–X**	**Cu···Cu**	**Cu–X–X**	**I–Cu–I**	**I–Cu–X**	**Cu–I–Cu**
1	2.6704(6)–2.7869(6)	1.905(4), 1.908(3), 1.909(4), 1.913(4)	1.146(5), 1.158(5)	2.4696(6), 2.4634(6)	170.1(3), 172.1(3), 173.6(3), 174.5(3)	98.074(17)–104.656(18)	109.02(11)–122.68(11)	53.370(15)–54.536(15)
2	2.6785(4), 2.7431(4), 2.7650(4)	1.907(2)	1.162(4)	2.4841(6)	179.1(3)	100.115(11), 100.350(12), 102.319(11)	119.27(7), 115.42(7), 116.41(7)	53.846(13), 54.274(12)
3	2.6574(5)–2.9262(5)	1.906(2), 1.918(3)	1.150(5), 1.160(5)	2.4818(6)	176.1(4), 177.6(4)	98.270(15)–104.914(16)	103.67(8)–124.75(8)	52.511(13), 54.029(14), 54.252(14)
4	2.6741(10)–2.7866(10)	1.911(6), 1.920(5)	1.149(11), 1.154(11)	2.4906(12)	177.8(8), 177.9(7)	98.99(3)–101.98(3)	110.97(19)–122.01(17)	55.46(3), 53.21(3), 54.29(3)

[a]X = disordered C/N.

3.2 X-ray crystallography

The iodocyanocuprate salts reported here are insoluble in common solvents. Therefore, X-ray quality crystals were prepared by heating unstirred mixtures identical to those used for the bulk products. Crystals were obtained and structures solved for all four $(RPy)_2[Cu_2I_3CN]$ complexes, **1**–**4**. All solved in monoclinic space groups, but none were isomorphic. The structure solution data and selected structural parameters for all compounds are presented in Tables 1 and 2, respectively. The four X-ray crystal structures of **1**–**4** are roughly isostructural, as is evident in Figures 1, 2, S1, and S2.

The iodocyanocuprate anion **1**–**4** each consists of trigonal bipyramid-shaped Cu_2I_3 clusters linked though C/N-positionally disordered cyano groups to produce an infinite and largely linear chains. Within the Cu_2I_3 clusters pairs of copper atoms are linked together by trios of μ_2-I atoms. In the case of **1**, two CuI_3CN groups and four cations make up the crystallographically independent repeat unit. For **3** and **4**, one CuI_3CN group and two cations comprise the repeat unit, and for **2**, one half CuI_3CN group and a single cation fulfill this role. While compounds **2**–**4** show symmetrically disordered C/N positions each centred across a special position, compound **1** shows non-symmetrically disordered C/N positions that are nonetheless almost evenly distributed between C and N.

The dicopper(I) triiodide clusters are quite similar amongst compounds **1**–**4**, with Cu–I bond length ranges of 2.6704(6)–2.7869(6) Å, 2.6785(4)–2.7650(4) Å, 2.6574(5)–2.9262(5) Å, and 2.6741(10)–2.7866(10) Å, respectively. The Cu–X (X = disordered C/N) distance ranges are 1.905(4)–1.913(4) Å, 1.907(2) Å, 1.906(2)–1.918(3) Å, and 1.911(6)–1.920(5) Å for **1**–

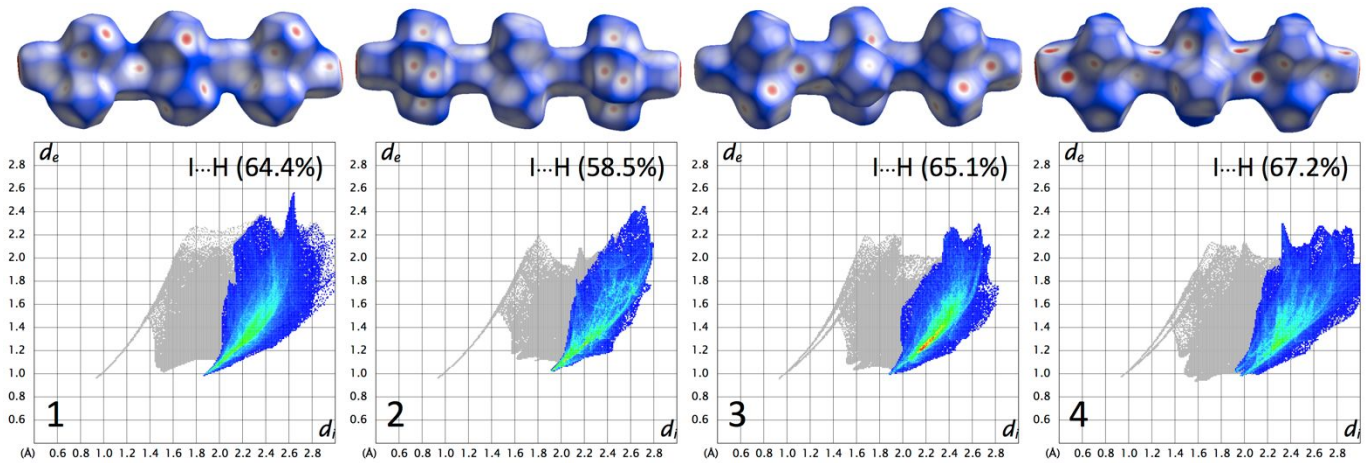

Figure 3. Hirshfeld surfaces and fingerprint plots from experimental structures of the close I···H atom contacts between the iodocyanocuprate anion and pyridinium cation in **1**–**4**. In all cases I···H hydrogen bonding dominates close contacts between ion pairs. Hirshfeld surface ranges: -0.2000 to +1.0000 au.

4, while the Cu···Cu distances are 2.4696(6) and 2.4634(6) Å, 2.4841(6) Å, 2.4818(6) Å, and 2.4906(12) Å, respectively. These intermetallic distances are remarkably short, being less than the value for copper metal (2.55 Å). Nevertheless, they are consistent with values noted in the previously reported series of $Cu_2I_3CN^{2-}$ salts.[9] The linearity of the anionic chains, as measured using end Cu atoms on three consecutive clusters along the chain, are 168.89°, 177.91°, 172.55°, and 172.57° respectively for **1**–**4**. Interestingly, when viewed along the chain alternating triangular trios of iodine atoms are staggered for **3** and **4**, but are eclipsed in the cases of **1** and **2**, see Figures 1, 2, S1, and S2. The pyridinium cations are ordered in all cases except that of **4**, in which case both cations were found to be disordered. One of these cations has all atoms disordered over two positions in nearly 1:1 ratio, while the other only shows disorder only in the butyl chain with a major and minor set of positions (see Figure S2). In all cases, the pyridinium cations are separated from the anionic chains. However, there are numerous close I···H–C interactions in each compound. In fact, only two iodine atoms lack close contacts to any cation: one of the six independent iodine atoms in compounds **1** and one of the three independent iodine atoms in **3**. In four structures, short I···H–C contacts are found involving both pyridyl and alkyl C–H units. Other non-covalent interactions include π···π stacking between two N6 pyridinium rings in **1** (centroid···centroid = 3.620 Å), and weak I···π interaction between I2 and the N2 pyridinium ring (I···centroid = 3.785 Å) in **2**.

3.3 Hirshfeld analysis

While the anionic iodocyanocuprate unit is nearly isomorphous across the series, differences in packing are realized as evident by variations in space group and unit cell parameters. Sterically dependent noncovalent interactions between ion pairs, controlled via pyridinium alkyl substituent, are the most likely cause for packing differences between **1**–**4**. Admittedly, Coulombic attractions are the primary drivers in assembly for these compounds, however, differences in noncovalent interactions such as hydrogen bonding are capable of subtly influencing assembly during crystallization, resulting in changes to photophysical properties. Crystallographically, we have already determined deviations in I···H–C contacts alongside observations of variable π···π and I···π interactions across the series. Thus, we have generated Hirshfeld surfaces of the iodocyanocuprate anions in **1**–**4** (Figure 3 and Electronic Supplementary Information) as a method to evaluate trends in noncovalent interactions for these compounds. Our findings are summarized in Table 3. In all cases hydrogen bonding between the triiodide motif and organic cation are dominant. The percent contribution of this interaction within the close atom···atom contacts range between 58.5% (compound **2**) and 67.2% (compound **4**). For the bulkier cations $PrPy^+$ and $BuPy^+$ in **3** and **4** these contacts occur between the hydrogens located on the R-group whereas for **1** and **2** occur with the hydrogens of the pyridinium ring. Hydrogen bonding with the cyano ligand account for the second greatest percent contribution and is relatively unchanged between compounds with an average percent contribution of 23.2%. Other noncovalent interactions between the pyridinium rings and iodide atoms, as measured by I···C contacts, are negligible except in the case of **2**. Here I···π interactions observed in the crystal structure are indicated by a bump of 7.4% percent contribution in close contacts. The findings from the Hirshfeld surfaces indicate that packing in **1**–**4** is largely driven by hydrogen bonding between the triiodide and pyridinium cation. This nature of this interactions, i.e. between the ring or the R-group, can be directed toward the R-group through use of bulky substituents. Additionally, the low incidence of interaction with the bridging cyano ligands points to steric hindrance by the halogen groups.

Table 3. Selected close atom···atom contacts with corresponding contribution.

	I···H	I···C	NC···H	CN···H
1	64.4%	2.1%	11.8%	10.5%
2	58.5%	7.4%	11.8%	11.8%
3	65.1%	2.1%	12.1%	11.0%
4	67.2%	0.5%	12.4%	11.4%

3.3 Photophysical behaviour

Compounds **1**–**4** present themselves in room light as yellow and orange in colour. Diffuse reflectance measurements, Figure 4 and Figure S14, show broad UV absorption bands that taper off in the mid-visible region around ~500 nm. Absorption edge energies are on the order of **2** > **1** > **3** > **4** at 2.48 eV, 2.42 eV, 2.36 eV, and 2.33 eV, respectively. The small absorption edge energies are indicative of semiconductive behaviour in agreement with the previously reported alkylimidazolium analogs.[9] It is noteworthy to point out that, generally speaking, the absorption edge red-shifts with increased contact between the organic cation and triiodide group. No correlation in band gap energy could be determined between a number of crystallographic parameters including Cu···Cu distance, chain angle, chain···chain distance, or R-group substituent.

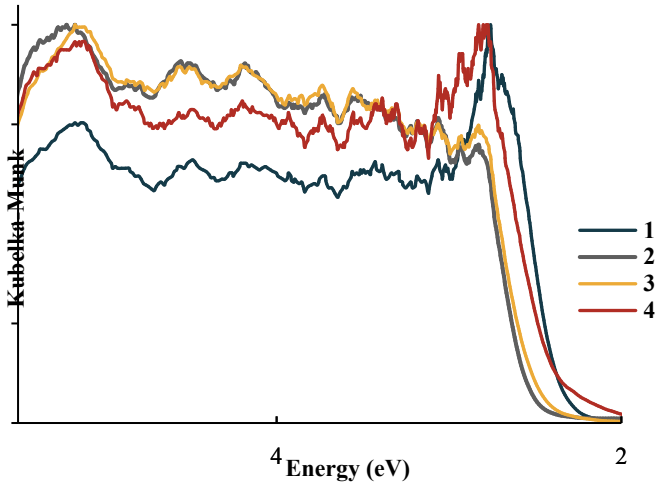

Figure 4. Kubelka-Munk function from diffuse reflectance spectra of microcrystalline samples of **1**–**4** at 298 K.

Photoluminescence measurements of **1**–**4** were performed between 298 K and 78 K, Figure 5. In all cases a single broad emission and excitation band is observed. Negligible differences between excitation bands are observed in **1**–**4** at both temperatures. The excitation bands span the UV and mid-visible region between 260 nm and ~530 nm with a maximum peak value at 400 nm. Fine peak resolution can be discerned at 454 nm and 468 nm, a feature we have seen with other iodocuprate(I)/pyridinium complexes.[10] With respect to emission, maximum peak energies generally follow the order **2** > **3** > **4** > **1**. Emission of **1** is lowest in energy, spanning from 565 nm past 850 nm, with a peak maximum at 725 nm (τ =962 ns). Upon cooling the band maximum does not shift, but instead band narrowing is observed as reduced emission intensity occurs at energies >622 nm and <850 nm. Complex **2** with an emission of 605 nm at 298 K (τ = 746 ns) undergoes a minor blue shift to 620 nm at 78 K and is accompanied by the appearance of a new shoulder at 535 nm. The appearance of this shoulder at low temperatures directs attention to the irregular shape of the 298 K emission band for **2**. Upon closer examination it becomes clear that a very minor shoulder is present around ~540 nm at room temperature. Complexes **3** and **4** both undergo red shifts when cooled to 78 K. For **3** the band shift occurs from 630 nm at 298 K (τ = 2,250 ns) to 620 nm at 78 K. The red shift is more dramatic in **4** shifting from 660 nm at 298 K (τ= 921 ns) to 620 nm at 78 K.

While Cu(I) complexes containing either halogen or cyanide ligands are well known,[2,20] in **1**–**4** a complex combination of 1D mixed cyano/iodocuprate(I) chain exists, with the inclusion of close Cu···Cu distances and interactions with aromatic organic cations. Even for relatively simple cases, such as inorganic ionic networks and coordination polymers lacking aromatic ligands,

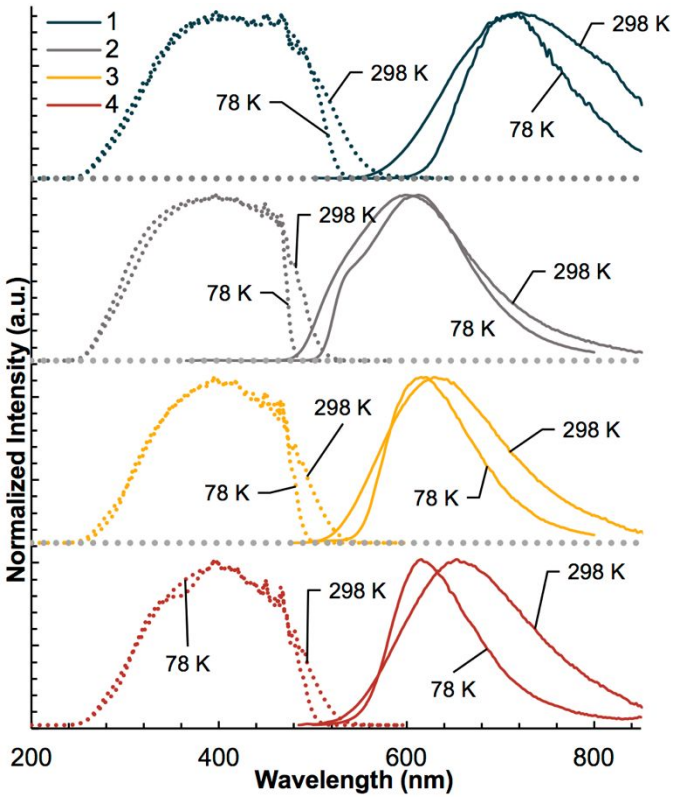

Figure 5. Photoluminescence of **1**–**4** at 298 K and 78 K. All emission profiles were obtained using an excitation value of 340 nm. Excitation profiles were obtained using the maximum λ_{em} value.

assignments of metal cluster charge transfer (MC) have been reported.[21] Inclusion of aromatic ligands such a substituted-pyridine or triphenylphosphite incorporates π^* acceptor molecular orbitals, leading to possible metal-to-ligand (MLCT) or mixed halide/metal-to-ligand (X/MLCT) charge transfer pathways.[22] Typically, band assignments can be accomplished through a combination of experimental observations including emission energy, temperature-dependent behavior, or lifetimes and literature precedent. However, the lack of spectroscopic background coupled with the extent of possible absorption and emission pathways, and subsequent rationalization of red shifting, makes assignment of bands difficult in the present series. The minor emission energy shifts observed between 298 K and 78 K help eliminate the possibility of a metal-centred transition upon photoexcitation. Metal-centred transitions typically exhibit significant red shifting of the emission band with decreasing temperatures. This shift, which has been well documented in iodocuprates,[22a] arises from stabilization of the metal halide cluster owing to increased overlap of Cu $3dz^2$ orbitals upon crystal contraction at low temperatures. The absence of this behaviour indicates that the excitation and

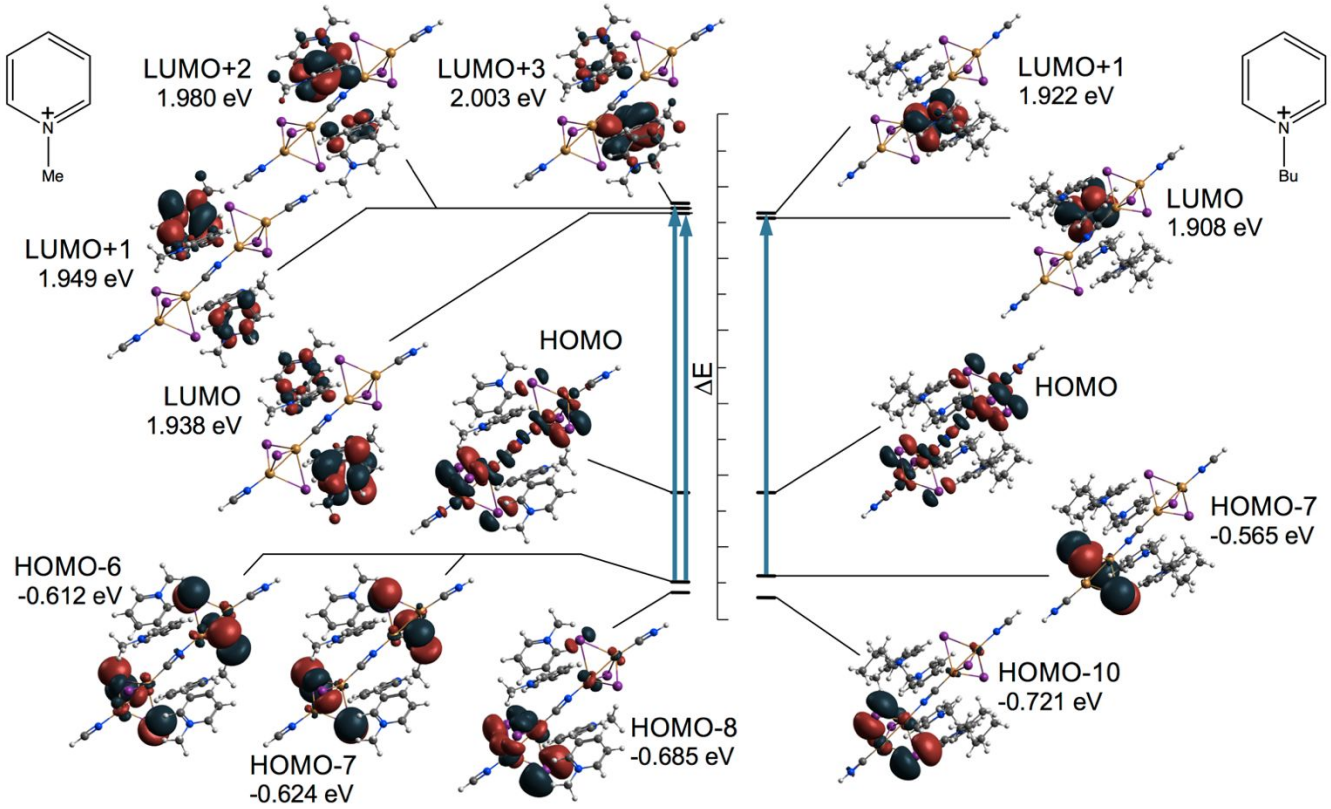

Figure 6. B3LYP/LANL2DZ Isodensity representations of the dominant transitions (>15%) of the lowest excited state for (left) **1** and (right) **4**.

emission pathway involves either a MLCT or X/MLCT transition, as has been suggested for the alkylimidazolium analogs.[9] With the spectroscopic data at hand, we were nevertheless unable to differentiate whether the photophysical bands observed are attributed to a MLCT or X/MLCT transition. Thus, we have utilized DFT and TD-DFT quantum calculations to visualize the photoinduced electronic transitions and pinpoint band assignments.

To accurately model the experimental photophysical observations for **1**–**4**, cationic models of formula $(RPy)_4[Cu_4I_6CN_3]^+$ were developed (Electronic Supplementary Information). Careful consideration was paid to the coordination sphere of the Cu(I), including close Cu···Cu distances. Our models maintain the tetrahedral metal coordination sphere along with the close Cu···Cu distances with values ranging from 2.50929 Å and 2.59899 Å, both values being within the sum of the van der Waals radii. Termination of the $[Cu_2I_3(CN)]_\infty^{2-}$ chain was accomplished using a charge-balanced HCN or HNC group. There was good qualitative agreement between experimental and theoretical values, indicating that the ground state models were accurate in modeling the photophysics of **1**–**4**. TD-DFT calculations of **1**–**4** provide the energy of the lowest excited state and electronic transitions involved. We have shown the lowest excited state transitions of **1** and **4** in Figure 6; remaining transitions can be found in the Electronic Supplementary Information. For **1** the calculated lowest excited state occurs at a wavelength of 593 nm with a high oscillation value of 0.0206, in good agreement to the experimental absorption edge of 579 nm. As seen in Figure 6, for this transition the higher-lying occupied molecular orbitals involved (HOMO-6 and HOMO-7) consist of the Cu $3dz^2/x^2–y^2$ and I 6*p* atomic orbitals. No cyano ligand character is observed in this electron donating molecular orbital. The distribution of orbitals does not appear to favor one $[Cu_2I_3]^-$ cluster over another and generally appears delocalized across the iodocyanocuprate(I) chain. The electron-accepting low-lying unoccupied molecular orbitals (LUMO and LUMO+3) are strictly π* type in composition and localized to the pyridinium cations. On the other end of the structural series by cation, a similar electronic transition as that of **1** is observed for the TD-DFT calculated lowest excited state of **4**. TD-DFT predicts this transition to occur at 620 nm with an oscillation value of 0.0153 (660 nm experimental). Here the electronic transition almost exclusively occurs between the HOMO-7 and LUMO+1. As with **1**, the electron donating molecular orbital HOMO-7 consists of the Cu 3*d* and I 6*s* atomic orbitals, while the acceptor orbitals are pyridinium π* in nature. Nearly identical transitions are also predicted for **2** and **3** and can be found in the Electronic Supplementary Information. It becomes clear that these transitions proceed via a mixed halide/metal-to-ligand (X/MLCT) Cu $3dz^2/x^2–y^2$/I 6*p* → pyridinium π* charge transfer, and we have assigned the absorption and emission bands as such. By identifying the nature of the transition we are able to rationalize the absorption edge red shift observed in **1**–**4** as well as the strikingly low emission energy of **1**. As a major component of the electron donating orbitals, increased noncovalent interaction with the triiodide appears to result in stabilization between the I 6*s* and pyridinium π*, demonstrating tunability of absorption edge via careful selection of pyridinium substituent. Furthermore, since the π* is the final emitting

molecular orbital, the π···π stacking displayed by **1** must afford a stabilizing effect to this MO, effectively lowering its emission energy. The spectroscopic measurements and modelling show that absorption and emission energies for this class of compounds are predominantly cation centered and implies that noncovalent interactions via pyridinium substituent can be used as a method to tune photophysical properties.

Conclusions

We have reported on a series of iodocyanocuprate(I) anions charged balanced by alkyl-substituted pyridinium cations, RPy^+ (R = Me, Et, Pr, Bu). Crystal structures of all four compounds feature triangular Cu_2I_3 clusters linked though C/N-positionally disordered cyano groups to produce infinite and essentially linear chains. Isolated 1D chains are parallel to one another and are linked via hydrogen bonded cations. Of particular note are close Cu···Cu distances between metal centres. Complexes **1**–**4** are photoluminescent upon irradiation with UV light. Photophysical measurements performed on solid samples reveal broad UV-visible absorption bands with absorption edge energies comparable to other semiconductors. While the excitation profile is nearly identical between all four complexes, the absorption and emission energies are dependent on choice cation and degree of noncovalent interaction with the triiodide. DFT and TD-DFT calculations, for the first time in this family of materials, definitively support a X/MLCT assignment to absorption and emission bands wherein the halocyanocuprate chain acts as an electron donor and the pyridinium π* acts as an electron acceptor.

Conflicts of interest

There are no conflicts to declare.

Acknowledgements

X-ray equipment was obtained with support from the NSF (CHE-0443345) and the College of William and Mary. We thank Prof. Christopher Cahill (George Washington Univ.) for the use of equipment and the Univ. of Maine Advanced Computing Group for their support and generous allocation of computing resources.

Notes and references

1 (a) W. Liu, K. Zhu, S. J. Teat, G. Dey, Z. Shen, L. Wang, D. M. O'Carroll, J. Li, *J. Am. Chem. Soc.* 2017, **139**, 9281–9290. (b) W. Fang, C. Tang, R. Chen, D. Jia, W. Jiang, Y. Zhang, Y. *Dalton Trans.* 2013, **42**, 15150–15158. (c) P. N. Bartlett, D. Cook, C. H. de Groot, A. L. Hector, R. Huang, A. Jolleys, G. P. Kissling, W. Levason, S. J. Pearce, G. Reid, *RSC Advances* 2013, **3**, 15645–15654.

2 T.-L. Yu, Y.-M. Guo, G.-X. Wu, X.-F. Yang, M. Xue, Y.-L. Fu, M.-S. Wang, *Coord. Chem. Rev.* 2019, **397**, 91–111.

3 C. H. Arnby, S. Jagner, I. Dance, *CrystEngComm* 2004, **6**, 257–275.

4 For recent examples see: (a) A. A. Petrov, V. N. Khrustalev, Y. V. Zubavichus, P. V. Dorovatovskii, E. A. Goodilin, A. B. Tarasov, *Mendeleev Commun.* 2018, **28**, 245–247. (b) G.-N. Liu, R.-Y. Zhao, H. Xu, Z.-H. Wang, Q.-S. Liu, M. Z. Shahid, J.-L. Miao, G. Chen, C. Li, *Dalton Trans.* 2018, **47**, 2306–2317. (c) X.-W. Lei, C.-Y. Yue, S. Wang, H. Gao, W. Wang, N. Wang, Y--D. Yin, *Dalton Trans.* 2017, **46**, 4209–4217. (d) J.-J. Shen, X.-X. Li, T.-L. Yu, F. Wang, P.-F. Hao, Y.-L. Fu, *Inorg. Chem.* 2016, **55**, 8271–8273. (e) P. Hao, Y. Qiao, T. Yu, J. Shen, F. Liu, Y. Fu, *RSC Advances* 2016, **6**, 53566–53572. (f) S.-L. Li, X.-M. Zhang, *Inorg. Chem.* 2014, **53**, 8376–8383. (g) J.-J. Zhao, X. Zhang, Y.-N. Wang, H.-L. Jia, J.-H. Yu, J.-Q. Xu, *J. Solid State Chem.* 2013, **207**, 152–157.

5 S.-L. Li, F.-Q. Zhang, X.-M. Zhang, *Chem. Commun.* 2015, **51**, 8062–8065.

6 G. A. Bowmaker, H. Hartl, V. Urban, *Inorg. Chem.* 2000, **39**, 4548−4554.

7 (a) S. Hibble, S. G. Eversfield, A. R. Cowley, A. M. Chippindale, *Angew. Chem., Int. Ed.* 2004, **43**, 628−630. (b) A. M. Chippindale, S. J. Hibble, A. R. Cowley, *Inorg. Chem.* 2004, **43**, 8040–8048.

8 X. Liu, G.-C. Guo, A.-Q.; Wu, L.-Z. Cai, J.-S. Huang, *Inorg. Chem.* 2005, **44**, 4282−4286.

9 Y.-L. Zhang, R. Ding, S.-N. Li, Y.-C. Jiang, M.-C. Hu, Q.-G. Zhai, *Inorg. Chem.* 2017, **56**, 7161–7174.

10 A. M. Wheaton, M. E. Streep, C. M. Ohlhaver, A. D. Nicholas, F. H. Barnes, H. H. Patterson, R. D. Pike, *ACS Omega* 2018, **3**, 15281−15292.

11 SAINT PLUS: Bruker Analytical X-ray Systems: Madison, WI, 2001.

12 SADABS: Bruker Analytical X-ray Systems: Madison, WI, 2001.

13 (a) G. M. Sheldrick, *Acta Crystallogr., Sect. A* 2008, **64**, 112-122. (b) G. M. Sheldrick, *Acta Crystallogr. Sect. C* 2015, **71**, 3-8.

14 C. B. Hübschle, G. M. Sheldrick, B. Dittrich, *J. Appl. Cryst.* 2011, **44**, 1281-1284.

15 M. J. Frisch, G. W. Trucks, H. B. Schlegel, G. E. Scuseria, M. A. Robb, J. R. Cheeseman, G. Scalmani, V. Barone, B. Mennucci, G. A. Petersson, H. Nakatsuji, M. Caricato, X. Li, H. P. Hratchian, A. F. Izmaylov, J. Bloino, G. Zheng, J. L. Sonnenberg, M. Hada, M. Ehara, K. Toyota, R. Fukuda, J. Hasegawa, M. Ishida, T. Nakajima, Y. Honda, O. Kitao, H. Nakai, T. Vreven, J. A. Montgomery, J. E. Peralta, Jr., F. Ogliaro, M. Bearpark, J. J. Heyd, E. Brothers, K. N. Kudin, V. N. Staroverov, R. Kobayashi, J. Normand, K. Raghavachari, A. Rendell, J. C. Burant, S. S. Iyengar, J. Tomasi, M. Cossi, N. Rega, J. M. Millam, M. Klene, J. E. Knox, J. B. Cross, V. Bakken, C. Adamo, J. Jaramillo, R. Gomperts, R. E. Stratmann, O. Yazyev, A. J. Austin, R. Cammi, C. Pomelli, J. W. Ochterski, R. L. Martin, K. Morokuma, V. G. Zakrzewski, G. A. Voth, P. Salvador, J. J. Dannenberg, S. Dapprich, A. D. Daniels, O. Farkas, J. B. Foresman, J. V. Ortiz, J. Cioslowski, D. J. Fox, Gaussian 16, Revision B.01, Gaussian, Inc., Wallingford CT, 2016.

16 (a) A. D. Becke, *J. Chem. Phys.* 1993, **98**, 5648–5652. (b) C. Lee, W. Yang, R. G. Parr, *Phys. Rev. B* 1988, **37**, 785–789.

17 (a) T. H. Dunning, Jr., P. J. Hay, in Modern Theoretical Chemistry, Ed. H. F. Schaefer III, Vol. 3 (Plenum, New York, 1977) 1–28. (b) P. J. Hay, W. R. Wadt, *J. Chem. Phys.* 1985, **82**, 270–283. (c) W. R. Wadt, P. J. Hay, *J. Chem. Phys.* 1985, **82**, 284–298. (d) P. J. Hay, W. R. Wadt, *J. Chem. Phys.* 1985, **82**, 299–310.

18 M. D. Hanwell, D. E. Curtis, D. C. Lonie, T. Vandermeersch, E. Zurek, G. R. Hutchison, *J. Cheminform.* **2012**, *4*: 17.

19 M. J. Turner, J. J. McKinnon, S. K. Wolff, D. J. Grimwood, P. R. Spackman, D. Jayatilaka and M. A. Spackman, CrystalExplorer17 (2017). University of Western Australia. http://hirshfeldsurface.net.

20 (a) A. D. Nicholas, R. M. Bullard, A. M. Wheaton, M. Streep, V. A. Nicholas, R. D. Pike, H. H. Patterson. *Materials* 2019, **12**, 1211. (b) K. M. Henline, C. Wang, R. D. Pike, J. C. Ahern, B. Sousa, H. H. Patterson, A. T. Kerr, C. L. Cahill, *Cryst. Growth Des.* 2014, **14**, 1449−1458.
21 (a) S. Chen, J. Gao, J. Chang, Y. Li, C. Huangfu, H. Meng, Y. Wang, G. Xia, L. Feng, *ACS Appl. Mater. Interfaces* 2019, **11**, 17513–17520. (b) S.-L. Li, F.-Q. Zhang, X.-M. Zhang, *Chem. Commun.* 2015, **51**, 8062–8065.
22 (a) P. C. Ford, E. Cariati, J. Bourassa, *Chem. Rev.* 1999, **99**, 3625–3647. (b) Y. Okano, H. Ohara, A. Kobayashi, Y. Masaki, M. Kato, *Inorg. Chem.* 2016, **55**, 5227–5236. (c) F. Hou, M. Powell, D. B. Dougherty, R. D. Sommer, P. A. Maggard, *Cryst. Growth Des.* 2018, **18**, 5406–5416. (d) S. Perruchas, C. Tard, X. F. Le Goff, A. Fargues, A. Garcia, S. Kahlal, J.-Y. Saillard, T. Gacoin, J.-P. Boilot, *Inorg. Chem.* 2011, **50**, 10682–10692.

ARTICLE

TOC graphic: Reaction of RPyI, CuI, and CuCN produces anionic iodocyanocuprate(I) chains, $(RPy)_2[Cu_2I_3CN]$ which exhibit charge transfer that is influenced by the hydrogen bonding between the cation and the triiodide groups.